Extensions of EN 12354 vibration reduction index expressions by means of FEM calculations

Charlotte CRISPIN[1]; Lieven DE GEETERE[2]; Bart INGELAERE[3]

[1,2,3] Belgian Building Research Institute, Belgium

ABSTRACT

In this paper, a comparison is made between the measured and calculated vibration reduction indices (K_{ij}) and the engineering approximations in EN 12354-1. First, the existing expressions in EN 12354-1 for simple junctions of homogeneous elements are compared with a large data set of measured and calculated K_{ij} spectra. For more complex junctions, not in EN 12354-1, like junctions with cavity walls (H-junctions) and junctions with different surface masses for in-line elements, a large number of FEM calculations have been made, from which new engineering approximations are derived.

Keywords: Vibration reduction index, Flanking transmission, Prediction, FEM calculations I-INCE Classification of Subjects Number(s): 51.5

1. INTRODUCTION

The prediction model of airborne sound transmission between two rooms, presented in the European standard EN 12354-1 (2000) [1], is based on the acoustic performance of the different building elements involved. The precision of the prediction depends upon the accuracy of the input data. The vibration reduction index $K_{ij,}$ is one of these input data. It expresses, in a way, the attenuation of the power flow through a junction. A standard exists to measure the K_{ij} in laboratory [2] but there are also prediction formulas to estimate the K_{ij} presented in the annex E of the standard EN 12354-1 (2000).

At the BBRI laboratory, approximately 185 different K_{ij} have so far been measured according the standard ISO 10848 and compared to the prediction formulas. The measurements show an increase of the K_{ij} in function of the ratio of the surface mass faster than the one proposed by the predictions [3].

Therefore, this work examines whether the ratio of the characteristic moment-impedances ψ/χ (see Eq. 1) would not be more relevant in the prediction formula instead of the parameter $m'_{perp,i}/m'_i$ used in the standard 12354. Indeed, as explained by Cremer [4], it seems more logical that the attenuation of the vibration depends on this new ratio, as during a change of direction, only moments and angular velocities can participate in the energy transmission.

$$\frac{\psi}{\chi} = \sqrt[4]{\frac{m'_{\perp i} B^3_{\perp i}}{m'_i B^3_i}} \tag{1}$$

Where,

$m'_{\perp i}$ and m'_i are the surface masses of the plates perpendicular to plate *i* and plate *i* [kg/m²]

$B_{\perp i}, B_i$ are the bending stiffnesses of the plates perpendicular to plate *i* and plate *i* [N.m]

With,
$$B = \frac{Eh^3}{12(1-\mu^2)} \tag{2}$$

E is the Young modulus [N/m²]
h is the thickness [m]
μ is the Poisson ratio[-].
By neglecting the Poisson's ratio, this means that:

[1] charlotte.crispin@bbri.be
[2] lieven.degeetere@bbri.be
[3] bart.ingelaere@bbri.be

$$\frac{\psi}{\chi} = \left(\frac{\rho_{\perp i}}{\rho_i}\right)^{1/4} \left(\frac{h_{\perp i}}{h_i}\right)^{5/2} \left(\frac{E_{\perp i}}{E_i}\right)^{3/4} \quad (3)$$

The study below analyses the involvement of these ratios on the K_{ij} and proposes new prediction formulas with the variable ψ/χ.

A large number of FEM calculations have also been made to extend the existing formulas with new formulas for typical Belgian junctions as cavity walls.

2. NUMERICAL MODELLING

The software used for the numerical modelling is Actran 12. Actran is a general purpose finite element program for modelling sound propagation, transmission and absorption in an acoustic, vibro-acoustic or aero-acoustic context.

2.1 Models description

Three different junctions are modelled: a T-Junction, an X-junction and an H-junction. The currently finite element models are meshed in the 3D dimension. The size of the elements (max.0.1 m) is less than one sixth of the wavelength. For the parametric study, the density, the thickness and the Young modulus of each element are the variables.

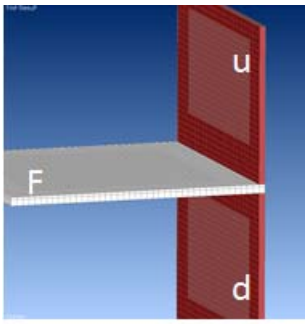

Figure 1 – Rigid T-junction
Wall (u) size: 2.5 mx4.28 m
Wall (d) size: 2.8 mx4.28 m
Floor (F) size: 4.31 mx4.28 m

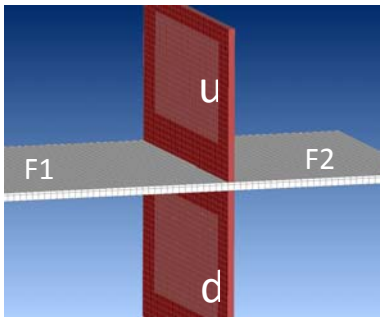

Figure 2 – Rigid X-junction
Wall (u) size: 2.5 mx4.28 m
Wall (d) size: 2.8 mx4.28 m
Floor (F1+F2) size: 7.4 mx4.28 m

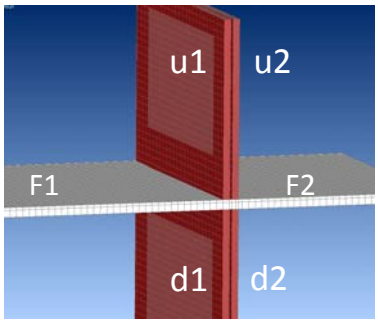

Figure 3 – Rigid H-junction
Walls (u1, u2) size: 2.5 mx4.28 m
Walls (d1, d2) size: 2.8 mx4.28 m
floor (F1+F2) size: 7.4 mx4.28 m
The cavity thickness between the walls is 4 cm.

2.2 Materials properties

The walls and the floor are modelled as Isotropic Solid Materials. A "Solid" component is used to model solid parts. Each node carries three degrees of freedom: the displacement components u_x, u_y and u_z.

For the parametric study:

- The Young Modulus varies from 2e+9 N/m² to 2.6e+10 N/m² (with 0.2 N/m² increments);
- The density varies from 400 kg/m³ to 2400 kg/m³ (with 200 kg/m³ increments);
- The thickness varies from 60 mm to 220 mm (with 20 mm increments);
- The damping is a constant: 0.01.

2.3 Boundary conditions

The lateral sides of the elements are clamped. The degree of freedom of the nodes on these lateral sides is therefore locked.

2.4 Analysis

Five dynamic point loads are applied successively on the walls and the floor. A radiating surface is determined on each face which stops at 0.4 m of walls (or floor) boundaries. A radiating surface is a set

of finite element faces on which the radiated acoustic power is calculated. Actran can compute various quantities on these surfaces as the Normal Mean Square Velocity, NMSV, [m²/s²] from 50 Hz to 3150 Hz. The values presented in this paper are however the mean vibration reduction index K_{ij}: the arithmetic average of K_{ij} within the frequency range from 200 Hz to 1250 Hz.

3. New engineering prediction formulas for K_{ij}

3.1 T-Rigid junctions

3.1.1 "In-line" transmission

The new prediction formula for this case is obtained by the adjustment of the coefficients *a*, *b*, *c*, of the Cremer's equation [4].

$$K_{du} = 10\lg\left(a + b\left(\frac{\psi}{\chi}\right) + c\left(\frac{\psi}{\chi}\right)^2\right) \ [\mathrm{dB}] \tag{4}$$

With, as a reminder (see Eq. 3),

$$\frac{\psi}{\chi} = \left(\frac{\rho_{\perp i}}{\rho_i}\right)^{1/4}\left(\frac{h_{\perp i}}{h_i}\right)^{5/2}\left(\frac{E_{\perp i}}{E_i}\right)^{3/4}$$

This means that the coefficients *a*, *b*, *c* have to give the best adjustment for the three following cases simultaneously:

$$1) \qquad (K_{du})_{\frac{h_{\perp i}}{h_i},\frac{E_{\perp i}}{E_i}} = 10\lg\left(a + b\left(\frac{\rho_{\perp i}}{\rho_i}\right)^{1/4} + c\left(\frac{\rho_{\perp i}}{\rho_i}\right)^{1/2}\right) \ [\mathrm{dB}] \tag{5}$$

Where the ratio $\frac{h_{\perp i}}{h_i}$ and $\frac{E_{\perp i}}{E_i}$ are constant

$$2) \qquad (K_{du})_{\frac{\rho_{\perp i}}{\rho_i},\frac{E_{\perp i}}{E_i}} = 10\lg\left(a + b\left(\frac{h_{\perp i}}{h_i}\right)^{5/2} + c\left(\frac{h_{\perp i}}{h_i}\right)^{5}\right) \ [\mathrm{dB}] \tag{6}$$

Where the ratio $\frac{\rho_{\perp i}}{\rho_i}$ and $\frac{E_{\perp i}}{E_i}$ are constant

$$3) \qquad (K_{du})_{\frac{\rho_{\perp i}}{\rho_i},\frac{h_{\perp i}}{h_i}} = 10\lg\left(a + b\left(\frac{E_{\perp i}}{E_i}\right)^{3/4} + c\left(\frac{E_{\perp i}}{E_i}\right)^{3/2}\right) \ [\mathrm{dB}] \tag{7}$$

Where the ratio $\frac{\rho_{\perp i}}{\rho_i}$ and $\frac{h_{\perp i}}{h_i}$ are constant

K_{ij} in function of the ratio of densities

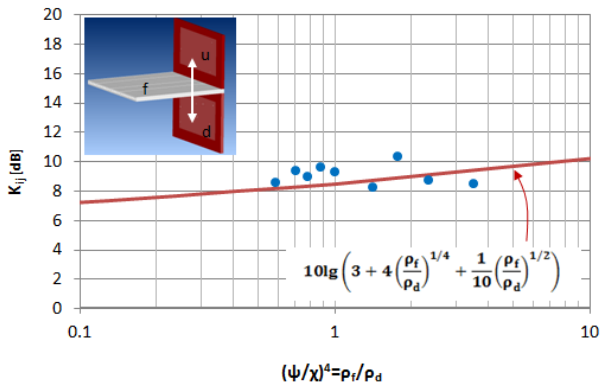

Figure 4 – Comparison between numerical results (●) and adjusted Cremer's equation (—).The thickness of walls and floor is constant: 140 mm. The Young

K_{ij} in function of the ratio of thicknesses

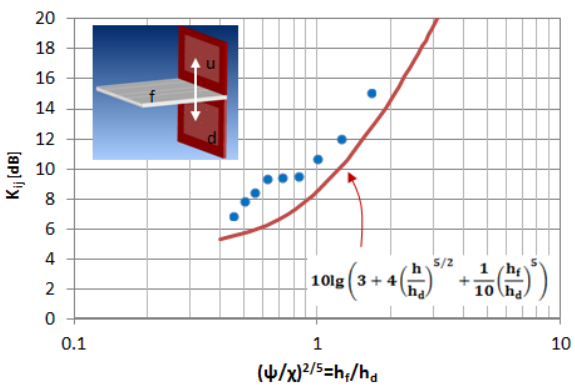

Figure 5 – Comparison between numerical results (●) and adjusted Cremer's equation (—). The density of walls and floor is constant: 1400

modulus is also constant: 1.0+10 N/m².

K_{ij} in function of the ratio of Young moduli

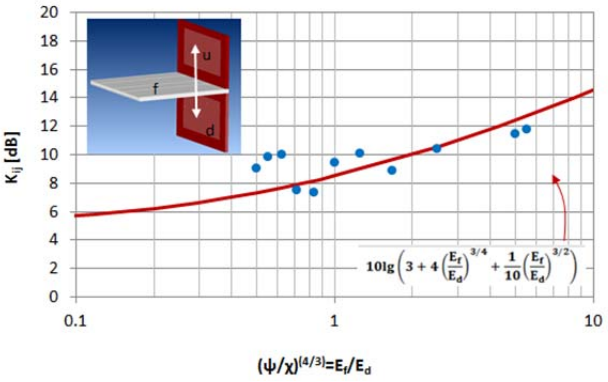

Figure 6 – Comparison between numerical results (●) and adjusted Cremer's equation (—). The density of walls and floor is constant: 1400 kg/m³. The thickness of the floor and walls is 140 mm.

kg/m³. The Young modulus is: 1.0+10 N/m².

The coefficients *a*, *b* and *c* which give the best adjustment for the three cases (Eq. 5, 6 and 7) simultaneously is: *a*=3, *b*=4 and *c*=1/10. The figures 4, 5 and 6 present the adjustment of the Cremer's equation on the FEM results.

The uncertainty on the FEM data's is attached to the modal behaviour of the plates.

At figure 4, we can observe that the K_{ij} increases monotonically with the density ratio. The low slope shows a light dependence of the K_{ij} with this ratio.

Figure 5: The curve increases also monotonically. The K_{ij} reaches 10.7 dB with FEM value and 8.5 dB with the fit curve when all the plates are identical.

Figure 6: As expected, the K_{ij} increases with the increasing ratio E_f/E_d. This ratio has a significant influence on the K_{ij}. The E modulus is often either a missing input data or a poorly estimated value but it cannot be neglected in the prediction formula for the K_{ij}. The predicted curve fits well with the FEM results.

3.1.2 "Corner" transmission

The new prediction formula for this case is obtained by the adjustment of the coefficients *d*, *e*, of the Cremer's equations [4].

$$K_{df} = 20\lg\left(\sqrt{d\left(\frac{\chi}{\psi}\right)} + \sqrt{\frac{1}{e}\left(\frac{\psi}{\chi}\right)}\right) \ [\mathrm{dB}] \tag{8}$$

With, as a reminder (see Eq. 3),

$$\frac{\psi}{\chi} = \left(\frac{\rho_{\perp i}}{\rho_i}\right)^{1/4}\left(\frac{h_{\perp i}}{h_i}\right)^{5/2}\left(\frac{E_{\perp i}}{E_i}\right)^{3/4}$$

This means that, as the "in-line transmission", the coefficients *d* and *e* have to give the best adjustment for the three following case simultaneously: $(K_{df})_{\frac{h_{\perp i}}{h_i},\frac{E_{\perp i}}{E_i}}$, $(K_{df})_{\frac{\rho_{\perp i}}{\rho_i},\frac{E_{\perp i}}{E_i}}$, $(K_{df})_{\frac{\rho_{\perp i}}{\rho_i},\frac{h_{\perp i}}{h_i}}$

The coefficients *d* and *e* which give the best adjustment for the three cases simultaneously is: *d*=1.4 and *e*=1.4. The figures 7, 8 and 9 present the adjustment of the Cremer's equation on the FEM results.

The ratio of densities

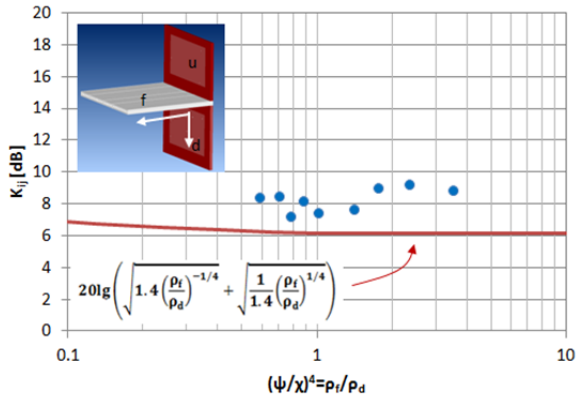

Figure 7 – Comparison between numerical results (●) and adjusted Cremer's equation (—). The thickness of walls and floor is constant: 140 mm. The Young modulus is also a constant: 1.0+10 N/m².

The ratio of thicknesses

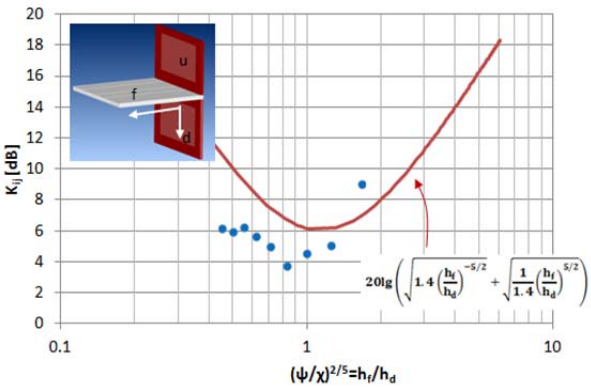

Figure 8 – Comparison between numerical results (●) and adjusted Cremer's equation (—). The density of walls and floor is constant: 1400 kg/m³. The Young modulus is: 1.0+10 N/m².

The ratio of Young moduli

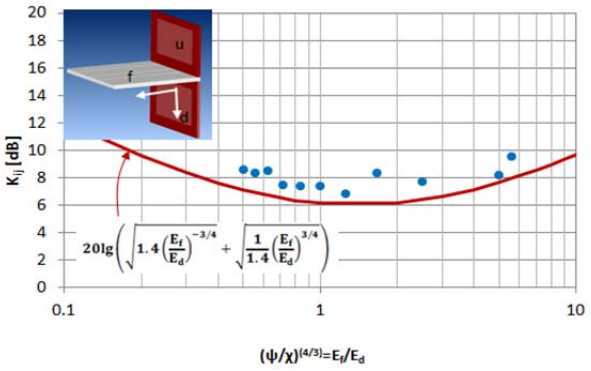

Figure 9 – Comparison between numerical results (●) and adjusted Cremer's equation(—).The density of walls and floor is constant: 1400 kg/m³. The thickness of the floor and walls is 140 mm.

Figure 7: The dependence of the K_{ij} with this ratio is insignificant. The prediction curve shows an underestimation for this case.

Figure 8: The vertical axis of symmetry of the predicted curve is found to h_f/h_d= 1.14. This is explained by Cremer [4] by the effect of two opposing tendencies: The total transmission efficiency is greatest for h_f=h_d but the fraction of that energy that is transmitted from the floor to wall *d* increases with increasing h_f/h_d. The FEM results show however a vertical axis of symmetry around 0.85. This fact still needs to be investigated.

Figure 9: The vertical axis of symmetry of the predicted curve is found at E_f/E_d= 1.57. This is explained by the effect of two opposing tendencies. The FEM results show the same tendency.

3.1.3 Validation

A large number of FEM calculations were computed for real masonry walls and compared to the new prediction formulas. Some measured K_{ij} are also plotted on the graphs.

"In-line" transmission

The new prediction formula proposed is:

$$K_{du} = 10\lg\left(3 + 4\left(\frac{\psi}{\chi}\right) + \frac{1}{10}\left(\frac{\psi}{\chi}\right)^2\right) \quad [\text{dB}] \tag{9}$$

With,

$$\frac{\psi}{\chi} = \sqrt[4]{\frac{m'_f B_f^3}{m'_d B_d^3}} \approx \left(\frac{\rho_f}{\rho_d}\right)^{1/4}\left(\frac{h_f}{h_d}\right)^{5/2}\left(\frac{E_f}{E_d}\right)^{3/4} \tag{10}$$

Figure 10 presents the comparison of the FEM results and measured results with the 12354 prediction while figure 11 presents a comparison of them with the new prediction (Eq.9).

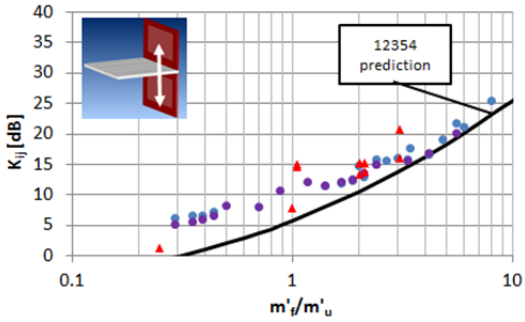

Figure 10 – K_{ij} in function of the ratio of surface mass: FEM results (● , ●) and measured results (▲) compared to the 12354 prediction (—)

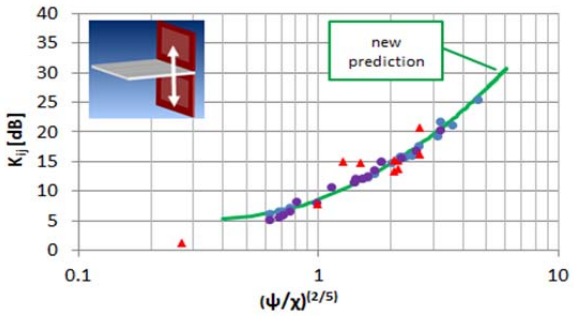

Figure 11 – K_{ij} in function of the ratio of characteristic moment-impedances: FEM results (● , ●) and measured results (▲) compared to the New prediction (—)

The purple bullets represent the K_{ij} in case the floor doesn't interrupt wall *u* and wall *d*. The blue bullets represent the K_{ij} in case the floor interrupts the walls. The results are similar. The new prediction (figure 11) shows a better adjustment with the FEM results and the measured results than the 12354 prediction (figure 10). The dispersion of the results is improved by expressing the results in function of the ratio of characteristic moment-impedances.

"Corner" transmission

The new prediction formula proposed is:

$$K_{df} = 20\lg\left(\sqrt{\frac{1.4\chi}{\psi}} + \sqrt{\frac{\psi}{1.4\chi}}\right) \quad [dB] \tag{11}$$

With, $$\frac{\psi}{\chi} = \sqrt[4]{\frac{m'_f B_f^3}{m'_d B_d^3}} \approx \left(\frac{\rho_f}{\rho_d}\right)^{1/4} \left(\frac{h_f}{h_d}\right)^{5/2} \left(\frac{E_f}{E_d}\right)^{3/4} \tag{12}$$

Figure 12 presents the comparison of the FEM results and measured results with the 12354 prediction while figure 13 presents a comparison of them with the new prediction (Eq.11). As above, the purple bullets represent the K_{ij} in case the floor doesn't interrupt wall *u* and wall *d*. The blue bullets represent the K_{ij} in case the floor interrupts the walls. The conclusions are similar to the "in-line" transmission conclusion: The new prediction (fig. 13) shows a better adjustment with the FEM results and the measured results than the 12354 prediction (fig. 12). Unfortunately, the coefficient of determination R^2 (which indicates how well the data fit with the new prediction) has not yet been calculated.

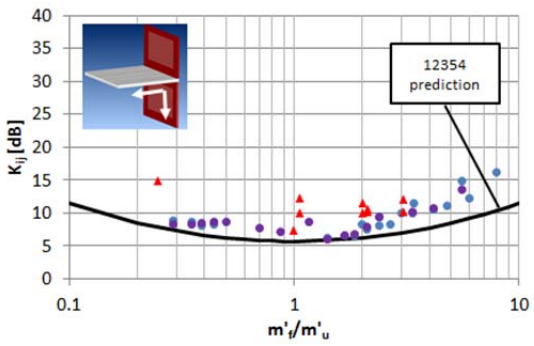

Figure 12 – K_{ij} in function of the ratio of surface mass: FEM results (● , ●) and measured results (▲) compared to the 12354 prediction (—)

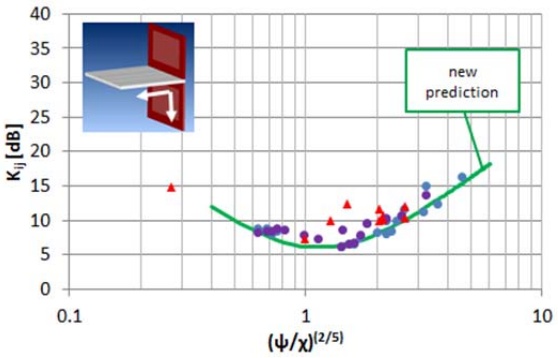

Figure 13 – K_{ij} in function of the ratio of characteristic moment-impedances: FEM results (● , ●) and measured results (▲) compared to the New prediction (—)

3.2 X-Rigid junction

"In-line" transmission

The new prediction formula proposed is:

$$K_{du} = 10\lg\left(5 + 5\left(\frac{\psi}{\chi}\right) + \frac{1}{2}\left(\frac{\psi}{\chi}\right)^2\right) \quad [dB] \tag{13}$$

With, $$\frac{\psi}{\chi} = \sqrt[4]{\frac{m'_f B_f^3}{m'_d B_d^3}} \approx \left(\frac{\rho_f}{\rho_d}\right)^{1/4}\left(\frac{h_f}{h_d}\right)^{5/2}\left(\frac{E_f}{E_d}\right)^{3/4} \tag{14}$$

Figure 14 presents the comparison of the FEM results and measured results with the 12354 prediction while figure 15 presents a comparison of them with the new prediction (Eq.13).

In figure 14, a measured value (3.32, 34.1) differs considerably from the 12354 prediction. This deviating value merits attention. This measured case had the following properties:

Table 1 – Properties of measured elements

	Floor	**Walls**
Density [kg/m³]	1575	1900
Thickness [m]	0.2	0.05
E [N/m²]	2.6e+10	6.62e+9

The ratio of the surface mass is then: 3.32

The ratio of the characteristic moment-impedances is (see Eq. 17):

$$\frac{\psi}{\chi} = \left(\frac{1575}{1900}\right)^{1/4}\left(\frac{0.2}{0.05}\right)^{5/2}\left(\frac{2.6e+10}{6.62e+9}\right)^{3/4} = 85.2$$

$$\Rightarrow \left(\frac{\psi}{\chi}\right)^{2/5} = 5.9$$

At figure 15 we can observe this point at (5.9, 34.1) and this fits well with the new predicted curve.

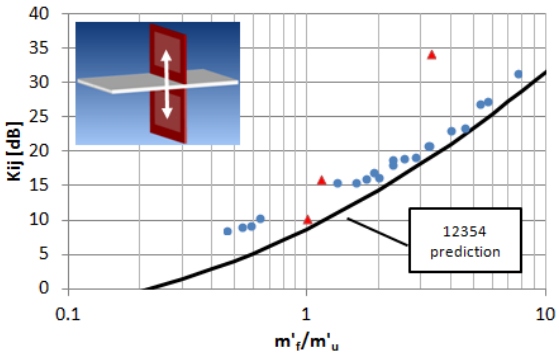

Figure 14 – K_{ij} in function of the ratio of surface mass: FEM results (●) and measured results (▲) compared to the 12354 prediction (—)

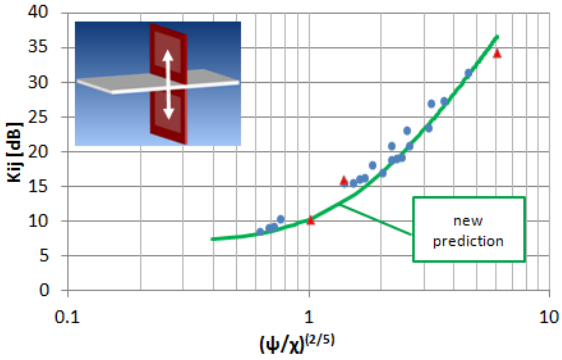

Figure 15 – K_{ij} in function of the ratio of characteristic moment-impedances: FEM results (●) and measured results (▲) compared to the New prediction (—)

"Corner" transmission

The new prediction formula proposed is:

$$K_{df} = 20\lg\left(\sqrt{\frac{2\chi}{\psi}} + \sqrt{\frac{\psi}{\chi}}\right) \quad [dB] \tag{15}$$

With,

$$\frac{\psi}{\chi} = \sqrt[4]{\frac{m'_f B_f^3}{m'_d B_d^3}} \approx \left(\frac{\rho_f}{\rho_d}\right)^{1/4} \left(\frac{h_f}{h_d}\right)^{5/2} \left(\frac{E_f}{E_d}\right)^{3/4} \tag{16}$$

Figure 16 presents the comparison of the FEM results and measured results with the 12354 prediction while figure 17 presents a comparison of them with the new prediction (Eq.15). Here, too, there is a good fit with the new prediction. It has to be noted that the prediction has been chosen to be secure.

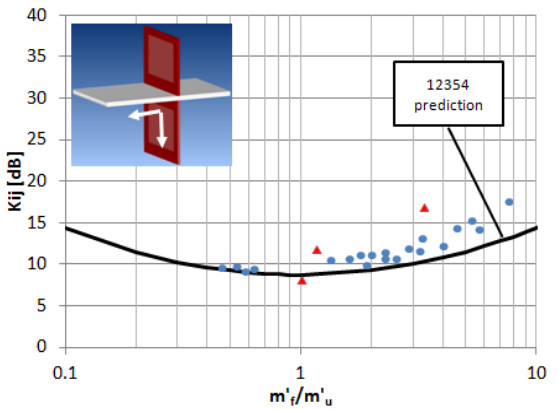

Figure 16 – K_{ij} in function of the ratio of surface mass: FEM results (●) and measured results (▲) compared to the 12354 prediction (—)

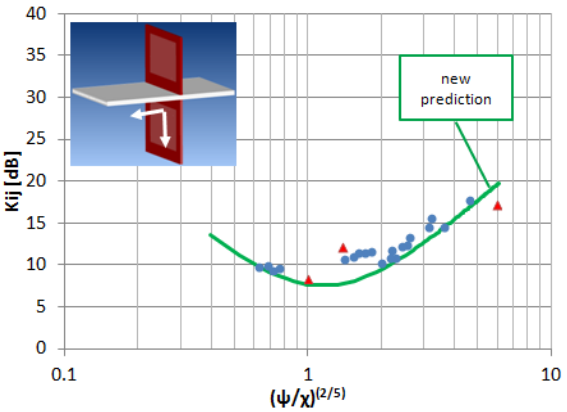

Figure 17 – K_{ij} in function of the ratio $(\psi/\chi)^{2/5}$: FEM results (●) and measured results (▲) compared to the New prediction (—)

3.3 H-Rigid junction

A large number of FEM calculations have also been made to extend the formulas for specific junctions such cavity walls. New prediction formulas are proposed for these H-Rigid junctions.

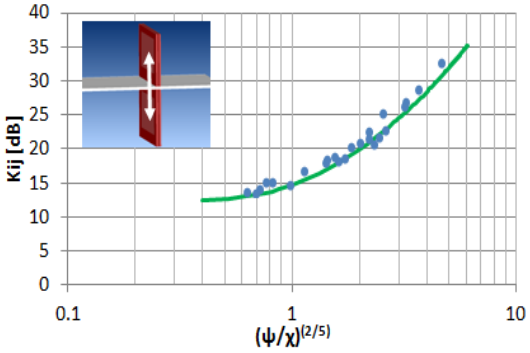

Figure 18 – K_{ij} in function of the ratio $(\psi/\chi)^{2/5}$ for the 'd1u1' transmission: FEM results (●) compared to the New prediction (Eq.17) (—)

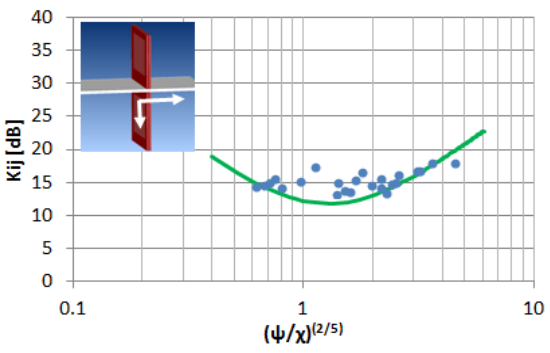

Figure 19 – K_{ij} in function of the ratio $(\psi/\chi)^{2/5}$ for the 'd1f2' transmission: FEM results (●) compared to the New prediction (Eq.18) (—)

$$K_{d1u1} = 10\lg\left(16 + 13\left(\frac{\psi}{\chi}\right) + \frac{1}{4}\left(\frac{\psi}{\chi}\right)^2\right) \text{ [dB]} \quad (17)$$

$$K_{d1f2} = 20\lg\left(\sqrt{\frac{7\chi}{\psi}} + \sqrt{\frac{2\psi}{\chi}}\right) \text{ [dB]} \quad (18)$$

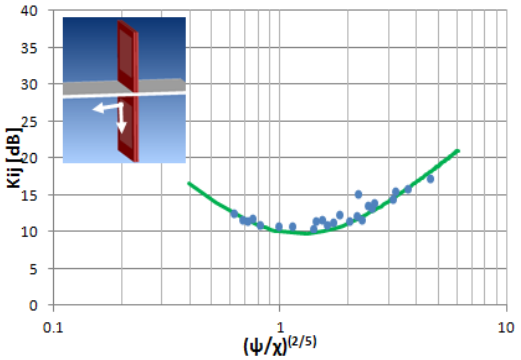

Figure 20 – K_{ij} in function of the ratio $(\psi/\chi)^{2/5}$ for the 'd1f1' transmission: FEM results (●) compared to the New prediction (Eq.19) (—)

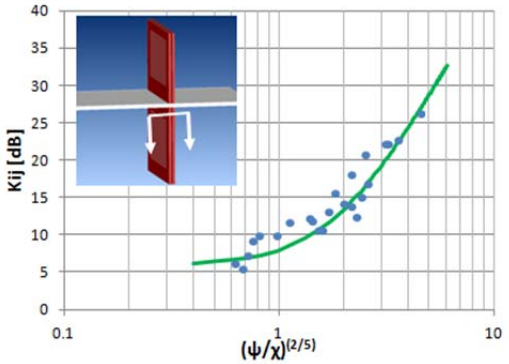

Figure 21 – K_{ij} in function of the ratio $(\psi/\chi)^{2/5}$ for the 'd1d2' transmission: FEM results (●) compared to the New prediction (Eq.20) (—)

$$K_{d1f1} = 20\lg\left(\sqrt{\frac{4\chi}{\psi}} + \sqrt{\frac{4\psi}{3\chi}}\right) \text{ [dB]} \quad (19)$$

$$K_{d1d2} = 10\lg\left(4 + 2\left(\frac{\psi}{\chi}\right) + \frac{1}{5}\left(\frac{\psi}{\chi}\right)^2\right) \text{ [dB]} \quad (20)$$

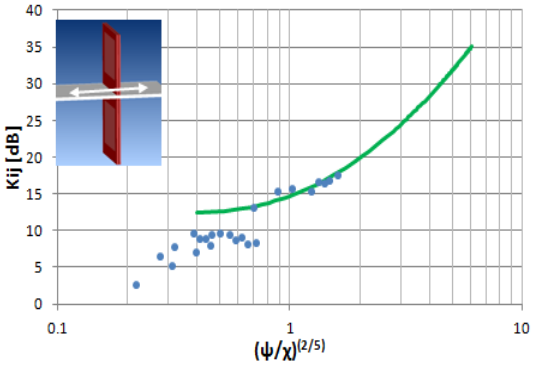

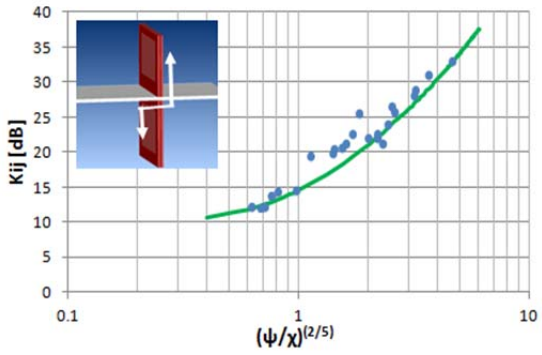

Figure 22 – K_{ij} in function of the ratio $(\psi/\chi)^{2/5}$ for the 'f1f2' transmission of a H-rigid junction: FEM results (●) compared to the New prediction (Eq.21) (—)

Figure 23 – K_{ij} in function of the ratio $(\psi/\chi)^{2/5}$ for the 'd1u2' transmission of a H-rigid junction: FEM results (●) compared to the New prediction (Eq.22) (—)

$$K_{f1f2} = 10\lg\left(16 + 13\left(\frac{\psi}{\chi}\right) + \frac{1}{4}\left(\frac{\psi}{\chi}\right)^2\right) \text{ [dB]} \quad (21)$$

$$K_{d1u2} = 10\lg\left(10 + 18\left(\frac{\psi}{\chi}\right) + \frac{1}{2}\left(\frac{\psi}{\chi}\right)^2\right) \text{ [dB]} \quad (22)$$

4. CONCLUSIONS

This work has shown that a best prediction of K_{ij} can be obtained using the ratio of the characteristic moment-impedances ψ/χ instead of the ratio surface mass $m'_{perp,i}/m'_i$. Indeed, as explained by Cremer, it seems more logical that the attenuation of the vibration depends on this new ratio as during a change of direction, only moments and angular velocities can participate in energy transmission.

The study has analysed the variation of the K_{ij} in function of this new ratio by FEM calculation and has derived new prediction formulas for T-Rigid junctions and X-Rigid junctions. These new predictions are validated with measured data.

A large number of FEM calculations have also been made to extend the formulas for specific junctions such cavity walls named H-Rigid junctions.

ACKNOWLEDGEMENTS

The authors wish to acknowledge the financial assistance of the Belgian Ministry of Economics Affairs.

REFERENCES

1. EN 12354-1 (2000) Building Acoustics — Estimation of acoustic performance of buildings from the performance of elements — Part 1: Airborne sound insulation between rooms;
2. ISO 10848-1 to 4 (2006, 2010). Acoustics - Laboratory measurement of the flanking transmission of airborne and impact sound between adjoining rooms;
3. Crispin C., Ingelaere B., Review of the empirical formulas for the prediction of the vibration reduction index Kij. BBRI Technical Report, DIVA2013/CCR003 (2013).
4. Cremer L., Heckl M., Ungar E.E., Structure-Borne Sound (Second Edition), Ed. Springer-Verlag (1988).